Hindawi
Wireless Communications and Mobile Computing
Volume 2024, Article ID 5445725, 12 pages
https://doi.org/10.1155/2024/5445725

Research Article

On the Performance of MMSE Channel Estimation in Massive MIMO Systems over Spatially Correlated Rician Fading Channels

Jorge F. Arellano[1], **Carlos Daniel Altamirano**[2], **Henry Ramiro Carvajal Mora**[2], **Nathaly Verónica Orozco Garzón**[2] and **Fernando Darío Almeida García**[3]

[1]*Departamento de Eléctrica, Electrónica y Telecomunicaciones, Universidad de las Fuerzas Armadas ESPE 171103, Sangolquí, Ecuador*
[2]*Faculty of Engineering and Applied Sciences, Telecommunications Engineering, Universidad de Las Américas (UDLA), Quito 170503, Ecuador*
[3]*John A. Paulson School of Engineering and Applied Sciences, Harvard University, Boston, MA 02134, USA*

Correspondence should be addressed to Henry Ramiro Carvajal Mora; henry.carvajal@udla.edu.ec

Received 10 November 2023; Revised 27 January 2024; Accepted 19 March 2024; Published 12 April 2024

Academic Editor: Antonio De Domenico

Massive multiple-input-multiple-output (M-MIMO) offers remarkable advantages in terms of spectral, energy, and hardware efficiency for future wireless systems. However, its performance relies on the accuracy of channel state information (CSI) available at the transceivers. This makes channel estimation pivotal in the context of M-MIMO systems. Prior research has focused on evaluating channel estimation methods under the assumption of spatially uncorrelated fading channel models. In this study, we evaluate the performance of the minimum-mean-square-error (MMSE) estimator in terms of the normalized mean square error (NMSE) in the uplink of M-MIMO systems over spatially correlated Rician fading. The NMSE allows for easy comparison of different M-MIMO configurations, serving as a relative performance indicator. Besides, it is an advantageous metric due to its normalization, scale invariance, and consistent performance indication across diverse scenarios. In the system model, we assume imperfections in channel estimation and that the random angles in the correlation model follow a Gaussian distribution. For this scenario, we derive an accurate closed-form expression for calculating the NMSE, which is validated via Monte-Carlo simulations. Our numerical results reveal that as the Rician $\mathcal{K}$-factor decreases, approaching Rayleigh fading conditions, the NMSE improves. Additionally, spatial correlation and a reduction in the antenna array interelement spacing lead to a reduction in NMSE, further enhancing the overall system performance.

1. Introduction

Massive multiple-input multiple-output (M-MIMO) technologies are pivotal for the evolution and deployment of fifth-generation (5G) and beyond-5G (B5G) wireless networks, as highlighted by recent research [1]. Specifically, M-MIMO enhances the reliability, security, and data transmission rates within wireless systems through the implementation of straightforward receiver processing techniques, as demonstrated in several relevant studies [2–6]. The concept of MIMO entails the integration of multiple antennas in both the transmission and reception elements of a wireless system. More specifically, M-MIMO characterizes a scenario where the base station (BS) boasts a substantially larger quantity of antennas in comparison to the number of user equipments (UEs) within the wireless system [7–9].

In wireless communication, the received signals undergo random attenuation when traversing the channel, a phenomenon known as fading, often attributed to the multiple-path propagation of transmitted signals [10, 11]. To capture the fading behavior, various statistical distributions have been proposed in the literature. One common alternative is the Rayleigh distribution, widely favored for its ability to emulate fading in non-line-of-sight (NLOS) multipath environments [12–14]. However, in line-of-sight (LOS) scenarios, alternative statistical distributions have been proposed. The Rician distribution stands out as a prominent choice for such environments, with the Rayleigh distribution considered a specific

case of the Rician distribution [15]. From a comprehensive literature review, it is evident that the performance of M-MIMO systems over Rician fading channels remains significantly less explored in comparison to Rayleigh fading scenarios. Moreover, within this less-explored domain, scenarios involving channel correlation in Rician fading channels xhave received even less attention despite their practical relevance [16–20].

Among the manifold advantages offered by M-MIMO technology, spatial diversity emerges as a pivotal feature that significantly enhances wireless system performance. However, harnessing this diversity hinges on the precise knowledge of channel state information (CSI) at the transceivers [21]. Consequently, the fading channel necessitates estimation through various approaches, including techniques such as maximum-likelihood (ML) estimation and minimum-mean-square-error (MMSE) estimation. Both strategies rely on a set of pilot symbols known to the receiver, a common practice elucidated in existing literature [3]. In particular, the MMSE estimator, often referred to as the linear MMSE (LMMSE) estimator, serves to minimize the Bayesian mean square error (MSE) between the actual and the estimated channel elements [22].

The presence of spatial correlation in fading, often influenced by the propagation environment or the geometry of the antenna array, introduces a level of coherence with practical scenarios in the way that fading affects signals arriving at different antennas [23]. This spatial correlation, although it may impact the diversity of M-MIMO systems, also holds the potential for advantageous outcomes when considering the pilot sequences employed for channel estimation. More specifically, the phenomenon of pilot contamination can be mitigated in such scenarios, as the orthogonality between pilot sequences is preserved to a greater extent compared to scenarios with no spatial correlation, where interference suppression becomes more challenging [24]. It is important to note that some research efforts have assumed a scenario where statistical independence exists between the fading processes affecting signals received at different antennas in the array, which, in practical terms, is not a realistic depiction of many real-world settings [16, 17].

In [25], a novel approach for inducing spatial correlation within the fading channel, which has a profound impact on the performance of M-MIMO systems, is introduced. This work delves into a comprehensive analysis of the spectral efficiency (SE), energy efficiency (EE), and hardware efficiency (HE) across various channel estimation strategies, all within the context of the system operating over correlated Rayleigh fading channels. Specifically, the study explores the performance of three prominent channel estimation methods: the MMSE, the element-wise MMSE (EW-MMSE), and the least-square (LS) estimators. In this context, the significance of channel spatial correlation takes center stage, particularly when dealing with the sizable antenna arrays typically encountered in M-MIMO systems. Thus, large arrays offer an impressive spatial resolution relative to the number of scattering clusters, making spatial correlation a pivotal factor in system performance.

Looking ahead, the future landscape of mobile cellular networks is poised to witness an increased proliferation of small cells in their deployment. These small cells are frequently positioned at lower elevations, such as lampposts, utility poles, and building rooftops. This strategic placement minimizes obstructions between the transmitting and receiving ends, consequently elevating the likelihood of establishing a direct LOS communication path. In these evolving scenarios, the traditional Rayleigh distribution, often used to model fading behavior, may not be the most suitable choice. Instead, alternative statistical distributions, such as the Rician fading model, prove to be more apt. They can provide invaluable insights for designers of M-MIMO systems, particularly in environments where LOS paths play a significant role in communication reliability and performance optimization.

In [26], a closed-form expression for SE is derived, taking into account a correlated Rician fading channel characterized by variations in the angles of arrival to the UEs, as perceived from the BS. This research demonstrates that, within M-MIMO systems, the sum-SE reaches its maximum when the number of antennas remains fixed. This line of investigation is extended in [27], where the performance of the LS and MMSE channel estimation methods are evaluated. This analysis focuses on the average mean squared error (AMSE) for M-MIMO systems, specifically considering uncorrelated Rician fading channels. Closed-form expressions for both the mean and variance of the AMSE are provided in this research. Furthermore, in their subsequent work [28], the authors delve into the realm of M-MIMO systems for internet-of-things (IoT) applications, particularly over uncorrelated Rician fading conditions. Here, they derive approximations for the expectation of the relative channel estimation error (RCEE) between IoT devices and the BS for both LS and MMSE estimation methods. Expanding upon this, in yet another publication [29], the authors explore the RCEE in the context of M-MIMO systems operating over uncorrelated Rician fading channels. In this scenario, the authors provide closed-form expressions for the probability density function (PDF) and cumulative distribution function (CDF) of RCEE. Notably, it is worth mentioning that none of these aforementioned studies consider the effects of imperfect channel estimation (ICE), leaving this aspect as a potential avenue for further research.

In [30, 31], the authors focus on a multicell M-MIMO system operating over spatially correlated Rician fading channels. These investigations delve into the statistical characteristics of three channel estimation methods: the MMSE, EW-MMSE, and LS techniques. They provide closed-form expressions to evaluate the SE. In a similar vein, in [32], it is considered a scenario involving cell-free M-MIMO, where spatial correlation in Rician fading channels is also taken into account. Notably, all these studies determine that the MMSE estimator consistently delivers the highest level of performance across various settings. Shifting the focus to the downlink (DL) transmission in a single-cell MIMO system over correlated Rician fading channels, in [33], the authors leverage the one-ring scattering model to replicate

the correlation effects in the transmission. This work also yields straightforward closed-form approximations for the ergodic rate.

Through a comprehensive review of existing literature, it has been identified a gap concerning the evaluation of the normalized mean square error (NMSE) [34] in MMSE estimation for M-MIMO systems operating over spatially correlated Rician fading channels. To the best of the authors' knowledge, no prior studies have specifically assessed the performance of the MMSE estimator in this context using the NMSE metric. This novel exploration is interesting for several reasons. First, NMSE acts as a pivotal relative performance indicator, facilitating straightforward comparisons among diverse M-MIMO configurations. Moreover, the analysis of NMSE offers advantages attributable to its normalization, scale invariance, provision of relative performance indications, and consistency across various scenarios. Furthermore, delving into the NMSE evaluation in the context of M-MIMO over Rician fading channels provides valuable insights into system behavior in realistic communication environments. This is because the Rician fading model, encompassing both LOS and multipath components, is pivotal for capturing the intricacies of different practical wireless transmission scenarios.

By the above, the performance of the uplink (UL) of a single-cell M-MIMO system over spatially correlated Rician fading is evaluated in this work in terms of the NMSE. Assuming that the random angles in the correlation model follow a Gaussian distribution and that ICE is performed at the receiver, an accurate closed-form expression to evaluate the NMSE of the MMSE channel estimator is derived, which is validated through Monte-Carlo simulations in different operating scenarios. Useful insights about the M-MIMO system performance are obtained from these results. The main contributions and findings of this work are summarized as follows:

(i) A precise closed-form expression for the calculation of the NMSE is derived. To validate the accuracy of this expression, extensive Monte-Carlo simulations are conducted across various representative scenarios.

(ii) Our findings underscore a noteworthy trend: as the Rician $\mathscr{K}$-factor diminishes, converging toward Rayleigh fading conditions, there is a discernible enhancement in NMSE. This improvement directly translates into an elevated system performance.

(iii) Our study also unveils the impact of spatial correlation and a reduction in antenna array interelement spacing on NMSE. Intriguingly, it is observed that these factors contribute to a reduction in NMSE, thereby improving the overall performance of the system.

These nuanced insights, supported by both analytical derivations and simulation results, offer interesting perspectives for the design and optimization of M-MIMO systems operating over spatially correlated Rician fading channels.

Table 1: Acronyms and abbreviations.

Abbreviation	Full form
5G	Fifth-generation
AMSE	Average mean squared error
AoA	Angle of arrival
AWGN	Additive white Gaussian noise
B5G	Beyond-5G
BS	Base station
CSI	Channel state information
CDF	Cumulative distribution function
DL	Downlink
EE	Energy efficiency
EW-MMSE	Element-wise minimum-mean-square-error
HE	Hardware efficiency
ICE	Imperfect channel estimation
IoT	Internet-of-things
i.i.d.	Independent and identically distributed
LMMSE	Linear minimum-mean-square-error
LOS	Line-of-sight
LS	Least-square
MMSE	Minimum-mean-square-error
M-MIMO	Massive multiple-input multiple-output
MSE	Mean square error
ML	Maximum-likelihood
NLOS	Non-line-of-sight
NMSE	Normalized mean square error
PDF	Probability density function
RCEE	Relative channel estimation error
SE	Spectral efficiency
SNR	Signal-to-noise ratio
UE	User equipment
ULA	Uniform linear array
UL	Uplink

The remainder of this work is organized as follows. Section 2 presents the system model and the procedure employed to generate spatially correlated fading channels. An expression to evaluate the NMSE for the MMSE channel estimator considering correlated Rician fading channels is derived in Section 3. Section 4 presents numerical results and discussions for some representative scenarios. Finally, Section 5 summarizes the main conclusions of this work.

Tables 1 and 2 provide a comprehensive list of abbreviations and notations utilized throughout this work, respectively.

2. System Model

Let us delve into the UL of a single-cell M-MIMO system. In this configuration, a BS is equipped with a uniform linear array (ULA) with M antennas, serving a group of K UEs, each equipped with a single antenna. These UEs are evenly distributed throughout the cell area. Considering this system model, this section presents a framework related to the received signals, along with pertinent details regarding the channel model.

Table 2: Symbols and notation.

Notation	Description
x	Scalar (lowercase letters)
$\mathbf{x}$	Vector (bold lowercase letters)
$\mathbf{X}$	Matrix (bold uppercase letters)
$f(x)$	PDF of the random variable x
$\mathrm{E}\{\cdot\}$	Expectation
$\mathrm{cov}\{\cdot\}$	Covariance
$(\cdot)^T$	Transpose
$(\cdot)^H$	Hermitian transpose
$\lvert\cdot\rvert$	Determinant
$\lVert\cdot\rVert_2$	Euclidean norm
$\mathrm{tr}(\cdot)$	Trace of a matrix
$\mathcal{N}(x, y)$	Circularly symmetric Gaussian random variable (x: mean, y: variance)
$\mathscr{CN}(x, y)$	Circularly symmetric complex Gaussian random variable (x: mean, y: variance)
$\boldsymbol{I}_x$	$x \times x$ identity matrix
$\mathbf{0}_x$	$x \times 1$ vector with zeros
$\mathbf{1}_x$	$x \times 1$ vector with ones
j	Imaginary unit ($\sqrt{-1}$)
d	ULA interelement spacing
K	Number of UEs in the M-MIMO system
M	Number of antennas in the ULA
P	Received power at the BS
$\mathbf{n}$	$M \times 1$ noise vector
$\mathbf{y}$	$M \times 1$ vector containing the received samples
$\mathbf{R}$	$M \times M$ spatial correlation matrix
$\mathbf{H}$	$M \times K$ channel matrix containing the small-scale fading
$\tilde{\mathbf{H}}$	$M \times K$ channel matrix containing correlated entries
$\tilde{\mathbf{Y}}$	Signal matrix used for channel estimation
$\tilde{\mathbf{y}}_k$	$M \times 1$ processed pilot signal vector for the kth UE
$h_{m,k}$	Channel gain for the mth antenna and the kth UE
$\rho_{m,k}$	NLOS component in the channel gain for the mth antenna and the kth UE
$\varrho_{m,k}$	LOS specular component in the channel gain for the mth antenna and the kth UE
σ_k^2	Variance of real Gaussian random variables in the NLOS component of the channel gain for the kth user
$\mathscr{K}_k$	Rician factor for the fading affecting the kth UE
θ_k	AoA for the kth UE
$\bar{\varphi}_n$	Angle of arriving of the planar wave at the ULA
λ	Wavelength
γ	SNR
$\boldsymbol{\Phi}$	$\tau \times K$ matrix containing K pilot sequences
$\boldsymbol{\Phi}_k$	kth pilot sequence of length τ
$\mathbb{Z}^+$	Set of positive integer numbers

2.1. Matrix Structure of the Received Signals. After a coherent detection stage (phase compensation) at the receiver, the vector of received samples, $\mathbf{y}$, can be written as the following column vector with M entries

$$\mathbf{y} = \sqrt{P}\tilde{\mathbf{H}}\,\mathbf{x} + \mathbf{n}, \tag{1}$$

where

$$\tilde{\mathbf{H}} = \mathbf{R}^{\frac{1}{2}}\mathbf{H}. \tag{2}$$

In Equations (1) and (2), P denotes the received power, the spatial correlation matrix $\mathbf{R}$, with dimensions $M \times M$, characterizes the overall propagation effects in terms of antenna gains, as well as the radiation patterns at both the transmitter and receiver. Moreover, $\mathbf{R}$ introduces the local dispersion over different angles. In particular, Gaussian, Laplacian, or uniform distributions can be assumed for generating these random angles [25]. In addition, $\mathbf{x}$ is a column vector whose entries are the symbols transmitted by the K UEs, $\mathbf{H}$ is the channel matrix with dimensions $M \times K$, containing the small-scale fading, and it can be written as

$$\mathbf{H} = \begin{bmatrix} h_{1,1} & h_{1,2} & \cdots & h_{1,K} \\ h_{2,1} & h_{2,2} & \cdots & h_{2,K} \\ \vdots & \vdots & \ddots & \vdots \\ h_{M,1} & h_{M,2} & \cdots & h_{M,K} \end{bmatrix}. \tag{3}$$

More details about the channel matrix and the spatial correlation matrix are given in the following subsection. Finally, in Equation (1), $\mathbf{n} = [n_1, n_2, \ldots, n_M]^T$ is a column vector whose M entries are independent and identically distributed (i.i.d.) additive white Gaussian noise (AWGN) samples, such that $n_m \sim \mathscr{CN}(0, \sigma_n^2), \forall m$.

2.2. Channel Model. Consider a Rician fading channel matrix, $\mathbf{H}$, whose (m, k)th entry is given by Cho et al. [11], Equation (3.52)

$$h_{m,k} = \sqrt{\frac{\mathscr{K}_k}{\mathscr{K}_k + 1}}\varrho_{m,k} + \sqrt{\frac{1}{\mathscr{K}_k + 1}}\rho_{m,k}, \tag{4}$$

where $\mathscr{K}_k$ is the Rician factor for the kth UE, which is defined by the ratio between the power of the LOS component and the power of the NLOS components [11]. In addition, $\varrho_{m,k}$ represents the LOS or specular components given by

$$\varrho_{m,k} = \exp\left(-\frac{\mathrm{j}2\pi d(m-1)\sin\theta_k}{\lambda}\right), \ \forall m, k, \tag{5}$$

where λ is the transmitted carrier wavelength, d denotes the normalized separation between antennas, and θ_k is the kth UE angle of arrival (AoA), which can be modeled as a uniformly distributed random variable into the interval $[-\pi/2, \pi/2)$ [17], Equation (3). Finally, in Equation (4), $\rho_{m,k}$ represents the NLOS components, such that,

$$\rho_{m,k} = g_{m,k,1} + \mathrm{j}g_{m,k,2}, \tag{6}$$

where $g_{m,k,i}, \sim \mathcal{N}(0, \sigma_k^2/2)$, for $i = 1, 2$ and $\forall m, k$.

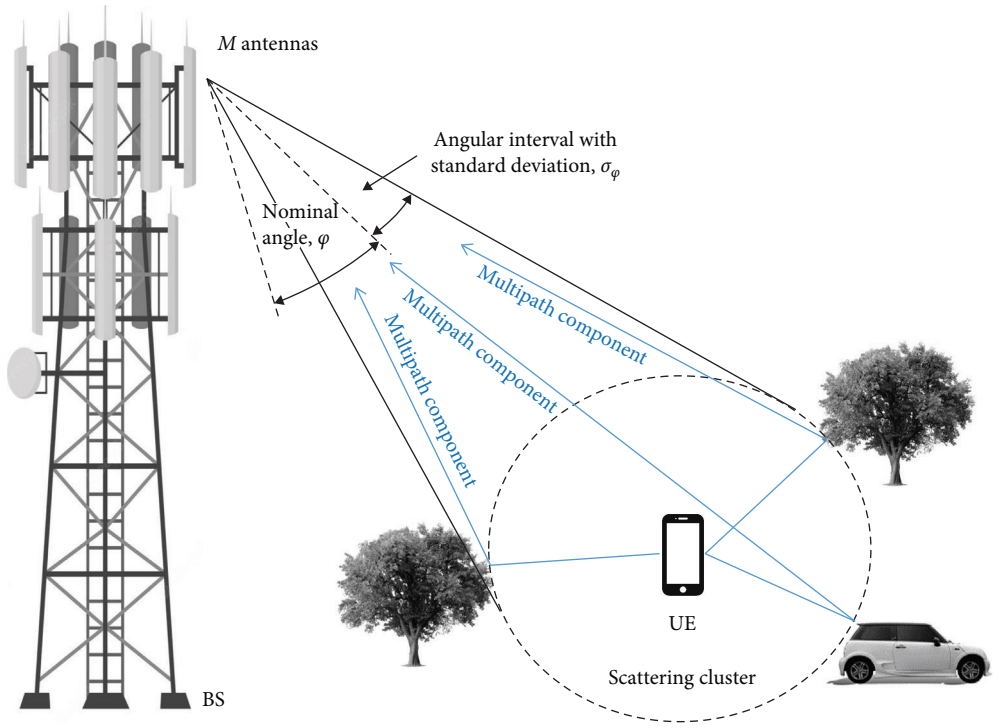

FIGURE 1: Propagation under a local scattering model.

Hereinafter, we consider a spatial correlation matrix **R** characterized by a Gaussian angular distribution [25], Section 2.6. In this particular model, the assumption is made that each multipath component generates a planar wave arriving at the antenna array from a distinct angle, as determined by

$$\bar{\varphi}_n = \varphi + \zeta, \tag{7}$$

where the nominal angle φ is deterministic, and ζ can be assumed as an aleatory deviation from φ, such that its standard deviation is σ_φ, as shown in Figure 1. This model is usually named as a local scattering model [35].

For a ULA, the entries of matrix **R** can be obtained as

$$r_{l,m} = \int_{-\infty}^{\infty} \exp\big(\quad \mathrm{j}2\pi d \sin(\bar{\varphi}_n)(l-m)\big) f(\bar{\varphi}_n) d\bar{\varphi}_n\,, \tag{8}$$

for $l = 1, 2, \ldots, M$ and $m = 1, 2, \ldots, M$, where d is the ULA interelement spacing and $f(\bar{\varphi}_n)$ is the PDF of $\bar{\varphi}_n$.

A practical use case for this system model could be in urban or suburban environments where a BS with a ULA serves multiple UEs. The even distribution of UEs in the cell area serves as a practical starting point for network planners in scenarios where an even coverage of cellular services is desired across the coverage area. Besides, this assumption in practical cellular network planning allows for a fair allocation of resources and enables the M-MIMO system to exploit spatial diversity effectively. In addition, the ULA stands out as a widely used and practical choice for antenna configurations in cellular networks due to its simplicity, ease of deployment, and compatibility with beamforming strategies [36].

The relevance of the system model for a practical use case can be further emphasized by considering the increasing density of nearby BSs, elevating the probability of LOS conditions between the UEs and the BS (This is due to the increasing use of higher frequencies in mobile cellular networks. As an example, 5G utilizes the 3.5 GHz band for initial deployments, resulting in a shorter coverage distance by each cell site. Therefore, the deployment of a greater number of BSs is required along coverage areas.). In such scenarios, the statistical Rician fading model aligns well with reality, capturing the dominance of LOS components amid the growing number of BSs. Moreover, in urban or suburban environments characterized by numerous surrounding objects, the choice of a Gaussian distribution for the local scattering model is pertinent [25]. This complements the system model by accounting for the multipath effects induced by the scattering of signals due to the presence of diverse objects, enhancing the model representation of complex propagation environments

3. NMSE Analysis for MMSE Channel Estimation

An expression to calculate the NMSE for MMSE channel estimation in M-MIMO systems over spatially correlated Rician fading channels is derived in this section.

For the channel estimation process, the UE transmits pilot sequences selected from the book, Φ, that is written as a $\tau \times K$ matrix given by

$$\begin{aligned}\boldsymbol{\Phi} &= [\boldsymbol{\Phi}_1, \boldsymbol{\Phi}_2, \ldots, \boldsymbol{\Phi}_K \quad] \\ &= \begin{bmatrix} \phi_{1,1} & \phi_{1,2} & \cdots & \phi_{1,K} \\ \phi_{2,1} & \phi_{2,2} & \cdots & \phi_{2,K} \\ \vdots & \vdots & \ddots & \vdots \\ \phi_{\tau,1} & \phi_{\tau,2} & \cdots & \phi_{\tau,K} \end{bmatrix},\end{aligned} \tag{9}$$

where the K pilot sequences of length τ are mutually orthogonal. Thus, a pilot sequence has a duration of τ symbol intervals. The kth pilot sequence is denoted by $\boldsymbol{\Phi}_k$ and each element of this sequence satisfies that $|\phi_{t,k}| = 1$, for $t = 1, 2, \ldots, \tau$ and $k = 1, 2, \ldots, K$, consequently, $\boldsymbol{\Phi}^H\boldsymbol{\Phi} = \tau\mathbf{I}_\tau$, and $\|\boldsymbol{\Phi}\|_2^2 = \tau$.

The pilot sequence length τ is limited by the coherence time, and this length should be greater or equal to K in order to avoid pilot contamination in the single cell M-MIMO system [31, 37]. Finally, the pilots' book can be generated by Walsh–Hadamard or discrete Fourier transform (DFT) matrices of dimension $\tau = 2^n$, for $n \in \mathbb{Z}^+$ [38, 39], or arbitrary dimensions [40], respectively.

Channel estimation through pilot signaling is the primary method for obtaining CSI. Hence, orthogonal pilot sequences of all UEs are known by the BS [41, 42].

Combining Equations (1) and (9), we obtain the received $M \times \tau$ signal matrix utilized for channel estimation as follows

$$\bar{\mathbf{Y}} = \sum_{k=1}^{K} \sqrt{P}\bar{\mathbf{h}}_k\boldsymbol{\Phi}_k^T + \mathbf{N}, \tag{10}$$

where $\bar{\mathbf{h}}_k$ denotes the kth column from the estimated channel matrix $\bar{\mathbf{H}}$, $\boldsymbol{\Phi}_k$ is the kth pilot sequence from the pilots book, and $\mathbf{N}$ is a $M \times \tau$ matrix containing the AWGN samples.

When we assume perfect orthogonality between the pilot sequences, interference is effectively eliminated. Consequently, the channel estimation process is solely influenced by noise. This simplifies the analysis of channel estimation, allowing for the use of a single value for parameter k in Equation (10) for analytical convenience.

In the channel estimation process for $\bar{\mathbf{h}}_k$, the BS must perform a multiplication or correlation operation between $\bar{\mathbf{Y}}$, as defined in Equation (10), and the pilot sequence $\boldsymbol{\Phi}_k$. This operation results in the processed received pilot signal, which is expressed as

$$\widetilde{\mathbf{y}}_k = \bar{\mathbf{Y}}\,\boldsymbol{\Phi}_k^* = \sum_{k=1}^{K} \tau\sqrt{P}\bar{\mathbf{h}}_k + \mathbf{N}\boldsymbol{\Phi}_k^*, \tag{11}$$

which has dimension $M \times 1$ and we have employed that $\boldsymbol{\Phi}_k^T\boldsymbol{\Phi}_k^* = \tau$. The processed received signal $\tilde{\mathbf{y}}_k$ contains sufficient statistics necessary for estimating $\bar{\mathbf{h}}_k$, as it retains all the information present in the originally received signal $\bar{\mathbf{Y}}$, a principle well established in the literature [22].

The MMSE estimator of $\bar{\mathbf{h}}_k$ is the vector $\widehat{\mathbf{h}}_k$ that minimizes $\mathrm{E}\{\|\bar{\mathbf{h}}_k - \widehat{\mathbf{h}}_k\|^2\}$. Hence, leveraging [25, Theorem 3.1], we can establish that the kth estimated channel vector in our scenario is attainable through

$$\widehat{\mathbf{h}}_k = \mathrm{cov}\{\bar{\mathbf{h}}_k\widetilde{\mathbf{y}}_k^H\}\mathrm{cov}\{\widetilde{\mathbf{y}}_k\widetilde{\mathbf{y}}_k^H\}^{-1}\widetilde{\mathbf{y}}_k. \tag{12}$$

In addition, since $\mathbf{N}\boldsymbol{\Phi}_k^* \sim \mathcal{CN}(\mathbf{0}_M, \tau\sigma_n^2\mathbf{I}_M)$, we have that

$$\begin{aligned}\mathrm{cov}\{\bar{\mathbf{h}}_k\widetilde{\mathbf{y}}_k^H\} &= \left(E\{\bar{\mathbf{h}}_k\widetilde{\mathbf{y}}_k^H\} - E\{\bar{\mathbf{h}}_k\}E\{\widetilde{\mathbf{y}}_k^H\}\right) \\ &= E\{\tau\sqrt{P}\bar{\mathbf{h}}_k\bar{\mathbf{h}}_kH + \bar{\mathbf{h}}_k\boldsymbol{\Phi}_k^T\mathbf{N}^H\} \\ &\quad - \tau\sqrt{P}E\{\bar{\mathbf{h}}_k\}E\{\bar{\mathbf{h}}_k^H\} \\ &= \tau\sqrt{P}\mathrm{cov}\{\bar{\mathbf{h}}_k\},\end{aligned} \tag{13}$$

and that

$$\begin{aligned}\mathrm{cov}\{\widetilde{\mathbf{y}}_k\widetilde{\mathbf{y}}_k^H\}^{-1} &= \left(E\{\widetilde{\mathbf{y}}_k\widetilde{\mathbf{y}}_k^H\} - E\{\widetilde{\mathbf{y}}_k\}E\{\widetilde{\mathbf{y}}_k^H\}\right)^{-1} \\ &= \left(\tau^2PE\{\bar{\mathbf{h}}_k\bar{\mathbf{h}}_kH\} - \tau^2PE\{\bar{\mathbf{h}}_k\}^2\right. \\ &\quad \left. + E\{\mathbf{N}\boldsymbol{\Phi}_k^*\boldsymbol{\Phi}_k^T\mathbf{N}^H\}\right)^{-1} \\ &= \left(\tau^2P\,\mathrm{cov}\{\bar{\mathbf{h}}_k\} + \tau\sigma_n^2\mathbf{I}_M\right)^{-1}.\end{aligned} \tag{14}$$

Thus, using Equations (13) and (14) and after some simplifications, Equation (12) can be rewritten as

$$\widehat{\mathbf{h}}_k = \sqrt{P}\mathrm{cov}\{\bar{\mathbf{h}}_k\}\boldsymbol{\Psi}\widetilde{\mathbf{y}}_k, \tag{15}$$

where

$$\boldsymbol{\Psi} = \left(\tau P\,\mathrm{cov}\{\bar{\mathbf{h}}_k\} + \sigma_n^2\mathbf{I}_M\right)^{-1}. \tag{16}$$

Hence, the vector containing the channel estimation error can be written as

$$\mathbf{e} = \bar{\mathbf{h}}_k - \widehat{\mathbf{h}}_k. \tag{17}$$

Due to the orthogonality principle [22], the channel estimate and the error are uncorrelated. Hence, from Equation (17), we can write the following covariance matrix

$$\begin{aligned}\mathrm{cov}\{\mathbf{e}\} &= E\left\{\left(\bar{\mathbf{h}}_k - \widehat{\mathbf{h}}_k\right)\left(\bar{\mathbf{h}}_k - \widehat{\mathbf{h}}_k\right)^H\right\} \\ &\quad - E\left\{\bar{\mathbf{h}}_k - \widehat{\mathbf{h}}_k\right\}E\left\{\left(\bar{\mathbf{h}}_k - \widehat{\mathbf{h}}_k\right)^H\right\} \\ &= E\{\bar{\mathbf{h}}_k\bar{\mathbf{h}}_kH\} - E\left\{\bar{\mathbf{h}}_k\widehat{\mathbf{h}}_k^H\right\} - E\left\{\widehat{\mathbf{h}}_k\bar{\mathbf{h}}_k^H\right\} \\ &\quad + E\left\{\widehat{\mathbf{h}}_k\widehat{\mathbf{h}}_k^H\right\} - E\left\{\bar{\mathbf{h}}_k - \widehat{\mathbf{h}}_k\right\}E\left\{\left(\bar{\mathbf{h}}_k - \widehat{\mathbf{h}}_k\right)^H\right\}.\end{aligned} \tag{18}$$

Appendix shows that Equation (18) can be simplified to

$$\mathrm{cov}\{\mathbf{e}\} = \mathrm{cov}\{\bar{\mathbf{h}}_k\} - \tau P\,\mathrm{cov}\{\bar{\mathbf{h}}_k\}\boldsymbol{\Psi}\,\mathrm{cov}\{\bar{\mathbf{h}}_k\}, \tag{19}$$

where

$$\mathrm{cov}\{\bar{\mathbf{h}}_k\} = \frac{\sigma_k^2}{\mathscr{K}_k + 1}\mathbf{R}. \tag{20}$$

Now, with the aid of [25, eq. (3.20)] and using Equations (19) and (20), the NMSE for the MMSE channel estimation in M-MIMO systems over correlated Rician fading can be obtained as

$$\begin{aligned}\mathrm{NMSE} &= \frac{\mathrm{tr}(\mathrm{cov}\{\mathbf{e}\})}{\mathrm{tr}\left(\mathrm{cov}\{\bar{\mathbf{h}}_k\}\right)}, \\ &= \frac{\mathrm{tr}\left(\mathbf{R} - \gamma\frac{\sigma_k^2}{\mathscr{K}_k+1}\mathbf{R}\left(\gamma\frac{\sigma_k^2}{\mathscr{K}_k+1}\mathbf{R} + \mathbf{I}_M\right)^{-1}\mathbf{R}\right)}{\mathrm{tr}(\mathbf{R})},\end{aligned} \tag{21}$$

where γ is the signal-to-noise ratio (SNR) at the receiver during pilot signaling, which is given by

$$\gamma = \frac{\tau P}{\sigma_n^2}. \tag{22}$$

Assuming that ζ follows a Gaussian distribution (angular distribution scenario), i.e., $\zeta \sim \mathscr{N}(0, \sigma_\varphi^2)$, from Equations (7) and (8), the entries of matrix $\mathbf{R}$ in Equation (27) can be obtained as

$$\begin{aligned}r_{l,m} = \frac{1}{\sqrt{2\pi}\sigma_\varphi}\int_{-\infty}^{\infty}&\exp\big(\quad \mathrm{j}2\pi d\sin(\varphi+\delta)(l-m)\big) \\ &\times\exp\left(-\frac{\delta^2}{2\sigma_\varphi^2}\right)d\delta,\end{aligned} \tag{23}$$

for $l = 1, 2, \ldots, M$ and $m = 1, 2, \ldots, M$. By considering that ζ is a very small angular deviation and using that $\sin(\varphi+\delta) = \cos(\varphi)\sin(\delta) + \sin(\varphi)\cos(\delta)$, and that $\sin(\zeta) \approx \zeta$ and that $\cos(\zeta) \approx 1$, Equation (23) can be approximated by

$$r_{l,m} \approx \exp\left(\mathrm{j}\alpha_{l,m} - \frac{1}{2}\left[\sigma_\varphi\alpha_{l,m}\cot\varphi\right]^2\right), \tag{24}$$

with

$$\alpha_{l,m} = 2\pi d(l-m)\sin\varphi, \tag{25}$$

where we have also employed that $\cot\varphi = \cos\varphi/\sin\varphi$.

As a consequence, $\mathrm{tr}(\mathbf{R})$ is obtained as

$$\begin{aligned}\mathrm{tr}(\mathbf{R}) &= \sum_{m=1}^{M}\exp\left(\mathrm{j}\alpha_{m,m} - \frac{1}{2}\left[\sigma_\varphi\alpha_{m,m}\cot\varphi\right]^2\right) \\ &= M,\end{aligned} \tag{26}$$

where we have used that $\alpha_{m,m} = 0$. With this result, Equation (21) can be finally rewritten as

$$\mathrm{NMSE} = 1 - \frac{\gamma}{M}\frac{\sigma_k^2}{\mathscr{K}_k+1}\mathrm{tr}\left(\mathbf{R}^2\left(\gamma\frac{\sigma_k^2}{\mathscr{K}_k+1}\mathbf{R} + \mathbf{I}_M\right)^{-1}\right), \tag{27}$$

where we have also used that $\mathrm{tr}(\mathbf{A}-\mathbf{B}) = \mathrm{tr}(\mathbf{A}) - \mathrm{tr}(\mathbf{B})$, $\mathrm{tr}(c\mathbf{A}) = c\,\mathrm{tr}(\mathbf{A})$, and the fact that the trace is invariant under circular shifts, i.e., $\mathrm{tr}(\mathbf{ABC}) = \mathrm{tr}(\mathbf{BCA}) = \mathrm{tr}(\mathbf{CAB})$.

An interesting observation is that the NMSE expression in Equation (27) remains independent of the angle θ_k. Furthermore, it is worth noting that as $\mathscr{K}_k$ tends toward infinity, the second term in Equation (27) approaches zero, resulting in the NMSE converging to 1. This outcome implies that a larger value of $\mathscr{K}$ corresponds to a heightened estimation error. Consequently, for a fixed number of antennas and a specific SNR, the most accurate channel estimation is achieved when dealing with Rayleigh fading channels, where $\mathscr{K}_k = 0$. These insights will be confirmed in the subsequent section.

Finally, for validating the derived expression for the NMSE, we consider the high SNR regime, i.e., $\gamma \to \infty$. In this case, Equation (27) can be reduced to

$$\begin{aligned}\mathrm{NMSE} &\approx 1 - \frac{\gamma}{M}\frac{\sigma_k^2}{\mathscr{K}_k+1}\mathrm{tr}\left(\mathbf{R}^2\left(\gamma\frac{\sigma_k^2}{\mathscr{K}_k+1}\mathbf{R}\right)^{-1}\right) \\ &\overset{(a)}{\approx} 1 - \frac{1}{M}\mathrm{tr}(\mathbf{R}) \\ &\overset{(b)}{\approx} 0,\end{aligned} \tag{28}$$

where in step (a), we have used that $\mathbf{A}\mathbf{A}^{-1} = \mathbf{I}$, that $(c\mathbf{A})^{-1} = c^{-1}\mathbf{A}^{-1}$, and that $\mathrm{tr}(c\mathbf{A}) = c\,\mathrm{tr}(\mathbf{A})$, and in step (b) we have used the result of Equation (26). Therefore, as indicated by Equation (28), achieving a low channel estimation error necessitates ensuring a high SNR, aligning with the expected outcome and thus substantiating the validity of our mathematical model.

4. Results and Discussions

This section features a presentation of numerical results across a variety of representative scenarios.

4.1. Parameters Setting. For the computations performed in this section, we employ a spatial correlation matrix $\mathbf{R}$ with a Gaussian angular distribution. According to the findings in [43], a suitable value for σ_φ in urban scenarios stands at 10°. Consequently, unless explicitly specified, this standard deviation is employed in generating the random variable ζ, as defined in Equation (7).

For the sake of simulations and without compromising generality, we have adopted a nominal angle of $\varphi = 50°$. Additionally, we assume that all radio paths experience fading channels with identical statistics, i.e., $\mathscr{K}_1 = \mathscr{K}_2 = \cdots = \mathscr{K}$ and $\sigma_1^2 = \sigma_2^2 = \cdots = 1/\sqrt{2}$.

Ultimately, as our derived expressions are applicable to both Rayleigh and Rician fading channels, we address both scenarios in the subsequent subsection containing numerical

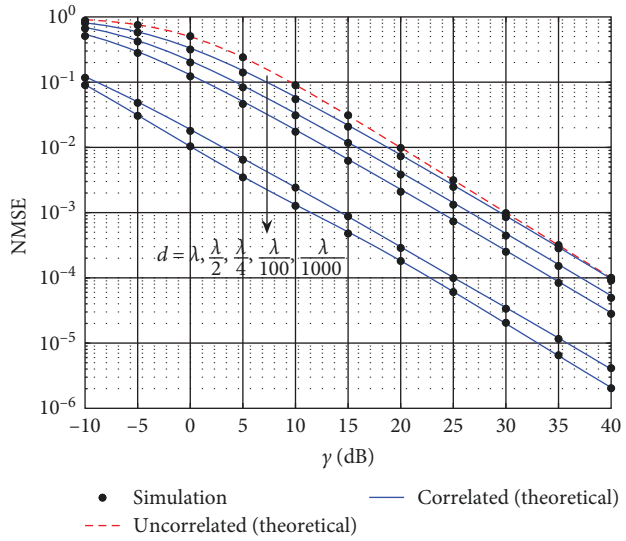

FIGURE 2: NMSE for MMSE channel estimation in an M-MIMO system as a function of the SNR and parameterized by different values of ULA interelement spacing, given in terms of λ, considering $M = 100$ antennas and a correlated Rayleigh fading channel.

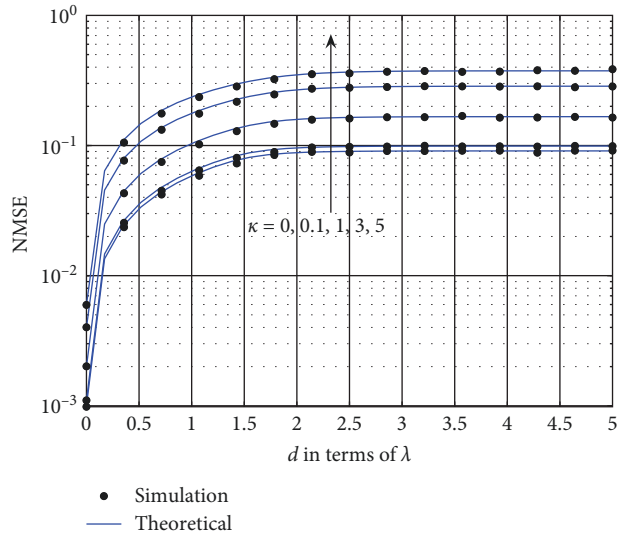

FIGURE 3: NMSE vs. the ULA interelement spacing, given in terms of λ, considering $\gamma = 10$ dB in the UL of an M-MIMO system where the BS employs $M = 100$ antennas across a range of correlated fading channels, parameterized by $\mathcal{K}$.

results. A total of 10^7 trials have been conducted to ensure statistical robustness in generating the simulated outcomes.

4.2. Numerical Results. In Figure 2, we present the NMSE plotted against the SNR for the UL of an M-MIMO system employing a configuration with $M = 100$ antennas, operating over correlated Rayleigh fading channels ($\mathcal{K} = 0$). The ULA interelement spacing, parameterized in terms of the signal wavelength λ, is varied to study its impact on NMSE. Within the figure, an appreciable alignment is observed between the simulation results and the theoretical outcomes, as computed using Equation (27). It is noteworthy that a decrease in the ULA interelement spacing corresponds to lower NMSE values. This phenomenon arises due to the heightened spatial correlation between antennas, enabling the MMSE estimator to achieve more precise channel estimates. Consequently, the uncorrelated scenario exhibits higher NMSE, underscoring the beneficial impact of channel correlation on enhanced channel estimation in M-MIMO systems. Furthermore, the NMSE exhibits a decreasing trend as the SNR rises. Specifically, a boost in the SNR of the M-MIMO system results in more accurate channel estimation, aligning with an expected outcome.

In Figure 3, we examine the relationship between the NMSE and the ULA interelement spacing expressed in terms of λ. These plots are conducted considering the UL of an M-MIMO system where the BS comprises 100 antennas. The system operates across a range of correlated fading channels, parameterized by the Rician factor $\mathcal{K}$, with a fixed SNR of $\gamma = 10$ dB. Notably, the results reveal that the average NMSE is directly proportional to the ULA interelement spacing, affirming the trend observed in the previous figure. It is essential to acknowledge that, in practical scenarios, a certain separation between antennas is practically unavoidable, driven by considerations such as the physical size of antennas and various

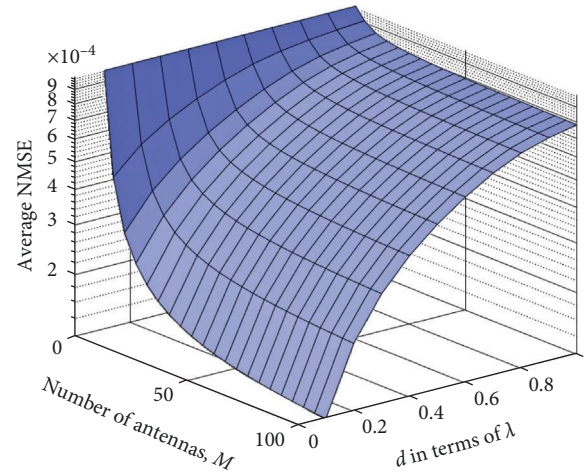

FIGURE 4: NMSE as a function of M and the ULA interelement spacing, given in terms of λ, considering an M-MIMO system over correlated Rician fading assuming $\mathcal{K} = 2$, and $\gamma = 30$ dB.

implementation factors. This separation between antennas is vital for achieving diversity in signal reception. Consequently, there exists an inherent trade-off in the design and implementation of M-MIMO systems, seeking a balance between preserving diversity and minimizing channel estimation errors. Additionally, it is evident from the results that as the Rician factor $\mathcal{K}$ increases, the average NMSE also experiences an increase. This outcome implies that with a constant SNR, the channel estimation error rises as the power of the LOS component grows, highlighting the intricacies of channel estimation in varying signal propagation conditions.

In Figure 4, the NMSE is explored as a function of the number of antennas at the receiver, denoted by N, and the ULA interelement spacing expressed in terms of λ. These

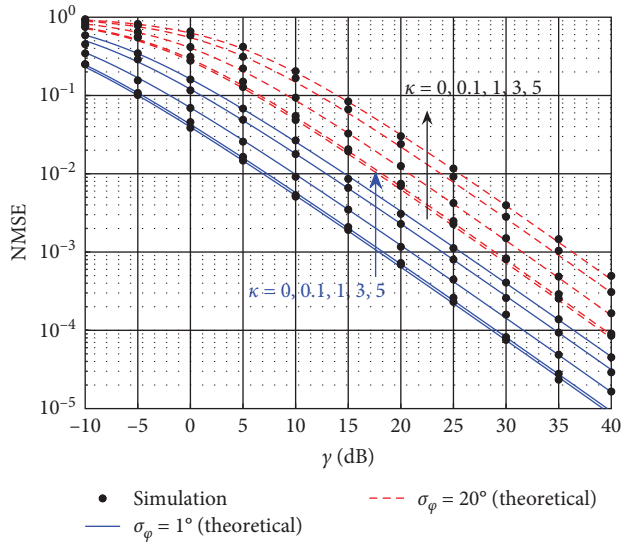

FIGURE 5: NMSE for an M-MIMO system vs. the SNR considering a ULA interelement spacing equal to $d = \lambda/2$ parameterized by $\mathscr{K}$ and σ_φ.

investigations are conducted within an M-MIMO system operating over correlated Rician fading channels, with parameters set at $\mathscr{K} = 2$ and an SNR of $\gamma = 30$ dB. A notable observation in this figure is the clear trend that as the number of antennas at the receiver increases, the NMSE approaches zero. Conversely, with an increase in ULA interelement spacing, the NMSE also rises. This outcome highlights the intriguing dynamic wherein a larger receiver antenna array contributes to more accurate channel vector estimation. However, it is imperative to bear in mind practical implementation considerations, as an excessive number of antennas or a significant separation between antennas can lead to infeasible scenarios. Consequently, the mathematical expression developed in this work serves as a tool for guiding the design of practical M-MIMO systems.

Finally, Figure 5 illustrates the behavior of the NMSE in an M-MIMO system concerning the SNR. The analysis involves a ULA interelement spacing of $d = \lambda/2$, and the parameter $\mathscr{K}$ is varied. In this figure, we also introduce modifications to the value of σ_φ. Notably, some slight deviations are observed between the theoretical results and the simulations, particularly in the case of $\sigma_\varphi = 20°$. This disparity arises from the increased values that the random variable ζ (refer to Equation (7)) can assume as σ_φ rises. As a result, the approximations employed in the calculation of Equation (24) introduce minor discrepancies between theoretical and simulated results. Nevertheless, these differences are nearly imperceptible. It is worth noting that, irrespective of the scenario, an increase in the SNR leads to a reduction in NMSE. This trend implies that the presence of a dominant LOS component significantly impacts the average NMSE of the MMSE estimator, which can be mitigated through SNR enhancement. Furthermore, the average NMSE tends to rise when σ_φ is elevated as a consequence of the greater standard deviation in the angle deviation within the correlation channel model. This heightened variability in the multipath signal introduces complexity to channel estimation, resulting in increased estimation errors. Nonetheless, such challenges can be ameliorated by increasing the SNR, as noticed in the numerical results.

All the previous results offer interesting insights into the practical implications for the design and implementation of M-MIMO systems. The investigation into the relationship between NMSE and ULA interelement spacing underscores the significance of optimizing the physical arrangement of antennas to exploit heightened spatial correlation and achieve more precise channel estimates. However, a trade-off exists in practical scenarios, as maintaining spatial diversity necessitates a certain separation between antennas. Additionally, the results highlight the impact of the Rician $\mathscr{K}$ factor on NMSE, emphasizing the need for tailored strategies in scenarios with varying LOS power. Furthermore, the observed trends affirm the importance of SNR for accurate channel estimation, suggesting that efforts to improve SNR can contribute to enhanced overall system performance. In essence, the findings guide M-MIMO system designers in balancing antenna configurations, considering practical constraints, and understanding signal propagation conditions for optimal channel estimation in real-world environments.

5. Conclusions

This work undertook an examination of the NMSE in the context of M-MIMO systems operating over correlated Rician fading channels. The correlated channel model was established by employing a correlation matrix that encapsulates the local angular dispersion across different angles of signal arrival. Within this system framework, we formulated an expression for assessing the NMSE, which hinges on several critical parameters, including the Rician $\mathscr{K}$ factor, the quantity of receiving antennas, their spatial separation, the SNR, and the characteristics of the spatial correlation matrix.

The numerical findings underscore several key insights. First, as the power of the LOS component intensifies, the NMSE increases. Conversely, heightened spatial correlation among signals and a reduction in the separation between antennas at the BS contribute to a decrease in NMSE. Similarly, an augmented number of antennas at the BS or an increase in SNR ensures a lower NMSE. Hence, the mathematical expression developed in this study offers a valuable tool for the design of M-MIMO systems, enabling the establishment of an optimal trade-off between implementation costs and channel estimation errors, which directly impacts system performance.

For future research endeavors, it is worthwhile to explore the NMSE in M-MIMO systems under different generalized channel models, such as κ-μ or η-μ. These models have gained attention as they aptly represent fading characteristics in millimeter-wave frequency scenarios, as evidenced in recent studies [44]. Furthermore, there is room for considering alternative statistical distributions to generate random angles that emulate the local dispersion within the correlated channel, potentially unveiling further insights into M-MIMO system performance over different scenarios. In particular, different distributions can influence the level of spatial correlation among antennas in the M-MIMO system. For

instance, in [45, Section 7.4], Laplace distributed deviations are presented, and in [33], uniformly distributed deviations are considered.

Appendix

Covariance Matrix Calculation for the Channel Estimation Error

In this appendix, the covariance matrix of the channel estimation error is simplified. For this, in the following, we calculate each term of Equation (18).

The first term in Equation (18) can be obtained as

$$\begin{aligned} E\{\bar{\mathbf{h}}_k\bar{\mathbf{h}}_k^H\} &= \operatorname{cov}\{\bar{\mathbf{h}}_k\} + E\{\bar{\mathbf{h}}_k\}E\{\bar{\mathbf{h}}_k^H\} \\ &= \operatorname{cov}\{\bar{\mathbf{h}}_k\} + E\{\bar{\mathbf{h}}_k\}^2. \end{aligned} \tag{A.1}$$

Moreover, by considering Equation (15), the second term in Equation (18) can be calculated as [15]

$$\begin{aligned} E\left\{\bar{\mathbf{h}}_k\widehat{\mathbf{h}}_k^H\right\} &= E\{\bar{\mathbf{h}}_k(\tau P \operatorname{cov}\{\bar{\mathbf{h}}_k\}\boldsymbol{\Psi}\bar{\mathbf{h}}_k)^H\} \\ &\quad + E\{\bar{\mathbf{h}}_k(\sqrt{P}\operatorname{cov}\{\bar{\mathbf{h}}_k\}\boldsymbol{\Psi}\mathbf{N}\boldsymbol{\Phi}_k^*)^H\} \\ &= \tau P(\operatorname{cov}\{\bar{\mathbf{h}}_k\} + E^2\{\bar{\mathbf{h}}_k\})\boldsymbol{\Psi}^H\operatorname{cov}\{\bar{\mathbf{h}}_k\}^H. \end{aligned} \tag{A.2}$$

Since $\mathbf{R}$ is a Toeplitz matrix, we have that $(\operatorname{cov}\{\bar{\mathbf{h}}_k\})^H = \operatorname{cov}\{\bar{\mathbf{h}}_k\}$. Therefore, Equation (A.2) can be rewritten as

$$E\left\{\bar{\mathbf{h}}_k\widehat{\mathbf{h}}_k^H\right\} = \tau P(\operatorname{cov}\{\bar{\mathbf{h}}_k\} + E\{\bar{\mathbf{h}}_k\}^2)\boldsymbol{\Psi}\operatorname{cov}\{\bar{\mathbf{h}}_k\}. \tag{A.3}$$

By following a similar procedure, the third term in Equation (18) can be obtained as

$$\begin{aligned} E\left\{\widehat{\mathbf{h}}_k\bar{\mathbf{h}}_k^H\right\} &= E\{\sqrt{P}\operatorname{cov}\{\bar{\mathbf{h}}_k\}\boldsymbol{\Psi}\widetilde{\mathbf{y}}_k\bar{\mathbf{h}}_k^H\} \\ &= \tau P\operatorname{cov}\{\bar{\mathbf{h}}_k\}\boldsymbol{\Psi}(E\{\bar{\mathbf{h}}_k\}^2 + \operatorname{cov}\{\bar{\mathbf{h}}_k\}). \end{aligned} \tag{A.4}$$

The fourth and fifth terms in Equation (18) are obtained as Equations (A.5) and (A.6), respectively, which are located at the bottom of this page. Then, using Equations (A.1)–(A.6) in Equation (18) and after some manipulations and simplifications, the covariance matrix of the channel estimation error can be rewritten as Equation (19).

$$\begin{aligned} E\left\{\widehat{\mathbf{h}}_k\widehat{\mathbf{h}}_k^H\right\} &= E\{P\operatorname{Cov}\{\bar{\mathbf{h}}_k\}\boldsymbol{\Psi}\widetilde{\mathbf{y}}_k\widetilde{\mathbf{y}}_k^H\boldsymbol{\Psi}^H\operatorname{Cov}\{\bar{\mathbf{h}}_k\}^H\} \\ &= E\{\tau^2P^2\operatorname{Cov}\{\bar{\mathbf{h}}_k\}\boldsymbol{\Psi}\bar{\mathbf{h}}_k\bar{\mathbf{h}}_k^H\boldsymbol{\Psi}^H\operatorname{Cov}\{\bar{\mathbf{h}}_k\}^H + P\operatorname{Cov}\{\bar{\mathbf{h}}_k\}\boldsymbol{\Psi}\mathbf{N}\boldsymbol{\Phi}_k^*\boldsymbol{\Phi}_k^T\mathbf{N}^H\boldsymbol{\Psi}^H\operatorname{Cov}\{\bar{\mathbf{h}}_k\}^H\} \\ &= \tau^2P^2\operatorname{Cov}\{\bar{\mathbf{h}}_k\}\boldsymbol{\Psi}(\operatorname{Cov}\{\bar{\mathbf{h}}_k\} + E\{\bar{\mathbf{h}}_k\}^2)\boldsymbol{\Psi}\operatorname{Cov}\{\bar{\mathbf{h}}_k\} + \tau P\operatorname{Cov}\{\bar{\mathbf{h}}_k\}\boldsymbol{\Psi}\sigma_n^2\mathbf{I}_M\boldsymbol{\Psi}\operatorname{Cov}\{\bar{\mathbf{h}}_k\}. \end{aligned} \tag{A.5}$$

$$\begin{aligned} E\left\{\left|\left(\bar{\mathbf{h}}_k - \widehat{\mathbf{h}}_k\right)^H\right|^2\right\} &= (E\{\bar{\mathbf{h}}_k\} - \tau P\operatorname{Cov}\{\bar{\mathbf{h}}_k\}\boldsymbol{\Psi}E\{\bar{\mathbf{h}}_k\})(E\{\bar{\mathbf{h}}_k^H\} - \tau PE\{\bar{\mathbf{h}}_k^H\}\boldsymbol{\Psi}^H\operatorname{Cov}\{\bar{\mathbf{h}}_k\}^H) \\ &= E\{\bar{\mathbf{h}}_k\}^2 - \tau PE\{\bar{\mathbf{h}}_k\}^2\boldsymbol{\Psi}^H\operatorname{Cov}\{\bar{\mathbf{h}}_k\}^H - \tau P\operatorname{Cov}\{\bar{\mathbf{h}}_k\}\boldsymbol{\Psi}E\{\bar{\mathbf{h}}_k\}^2 \\ &\quad + \tau^2P^2\operatorname{Cov}\{\bar{\mathbf{h}}_k\}\boldsymbol{\Psi}E\{\bar{\mathbf{h}}_k\}^2\boldsymbol{\Psi}^H\operatorname{Cov}\{\bar{\mathbf{h}}_k\}^H \\ &= E\{\bar{\mathbf{h}}_k\}^2 - \tau PE\{\bar{\mathbf{h}}_k\}^2\boldsymbol{\Psi}\operatorname{Cov}\{\bar{\mathbf{h}}_k\} - \tau P\operatorname{Cov}\{\bar{\mathbf{h}}_k\}\boldsymbol{\Psi}E\{\bar{\mathbf{h}}_k\}^2 \\ &\quad + \tau^2P^2\operatorname{Cov}\{\bar{\mathbf{h}}_k\}\boldsymbol{\Psi}E\{\bar{\mathbf{h}}_k\}^2\boldsymbol{\Psi}\operatorname{Cov}\{\bar{\mathbf{h}}_k\}. \end{aligned} \tag{A.6}$$

In Equation (19), considering that $\bar{\mathbf{h}}_k = \mathbf{R}^{\frac{1}{2}}\mathbf{h}_k$ like in Equation (2), the covariance matrix of $\bar{\mathbf{h}}_k$ is obtained as

$$\begin{aligned} \operatorname{cov}\{\bar{\mathbf{h}}_k\} &= \mathbf{R}^{\frac{1}{2}}E\{\mathbf{h}_k\mathbf{h}_k^H\}(\mathbf{R}^{\frac{1}{2}})^H \\ &\quad - \mathbf{R}^{\frac{1}{2}}E\{\mathbf{h}_k\}E\{\mathbf{h}_k^H\}(\mathbf{R}^{\frac{1}{2}})^H. \end{aligned} \tag{A.7}$$

In addition, we have that

$$E\{\mathbf{h}_k\mathbf{h}_k^H\} = E\left\{\begin{bmatrix} h_1h_1^* & h_1h_2^* & \cdots & h_1h_M^* \\ h_2h_1^* & h_2h_2^* & \cdots & h_2h_M^* \\ \vdots & \vdots & \ddots & \vdots \\ h_Mh_1^* & h_Mh_2^* & \cdots & h_Mh_M^* \end{bmatrix}\right\}, \tag{A.8}$$

such that

$$E\{h_a h_b^*\} = \begin{cases} \dfrac{\sigma_k^2 + \mathcal{K}_k}{\mathcal{K}_k + 1}, & a = b \\ \dfrac{\mathcal{K}_k}{\mathcal{K}_k + 1}, & a \neq b. \end{cases} \tag{A.9}$$

Thus, using Equations (A.8) and (A.9), that $E\{h_k\} = E\{h_k^*\} = (\frac{\mathcal{K}_k}{\mathcal{K}_k+1})^{-\frac{1}{2}}$, and after some manipulations, it is possible to show that Equation (A.7) can be rewritten as Equation (20).

Data Availability

This article does not involve the utilization of previous data. However, the authors have developed MATLAB algorithms for generating the plots presented in the paper. These algorithms served as tools for reproducing the results and visualizations discussed in the study. One of the base algorithms to generate Monte-Carlo simulations is shared in the following link: https://1drv.ms/f/s!AsRqANguaUiwheQBN-LzEULRqVZkhQ?e=GmPnFI.

Conflicts of Interest

The authors declare that they have no conflicts of interest.

Authors' Contributions

Conceptualization by J.F.A. and C.D.A.; methodology by J.F.A., C.D.A., and H.R.C.M.; software by J.F.A., C.D.A., and H.R.C.M.; validation by N.V.O.G., and F.A.G.; formal analysis by J.F.A., C.D.A., and H.R.C.M.; investigation by J.F.A., C.D.A., H.R.C.M., N.V.O.G., and F.A.G.; data curation by H.R.C.M.; writing of original draft preparation by J.F.A., C.D.A., and H.R.C.M.; writing of review and editing, H.R.C.M., N.V.O.G., and F.A.G.; visualization by J.F.A., and H.R.C.M.; supervision by C.D.A. All authors have read and agreed to the published version of the article.

Acknowledgments

The work of H.R.C. Mora and N.V.O. Garzón was supported by Universidad de Las Américas (Research project ERT.HCM.23.13.01). The work of F.D.A. García was supported by the São Paulo Research Foundation (FAPESP) (Grant Number 2022/13901-5).

References

[1] F. Salahdine, T. Han, and N. Zhang, "5G, 6G, and beyond: recent advances and future challenges," *Annals of Telecommunications*, vol. 78, pp. 525–549, 2023.

[2] L. Lu, G. Y. Li, A. L. Swindlehurst, A. Ashikhmin, and R. Zhang, "An overview of massive MIMO: benefits and challenges," *IEEE Journal of Selected Topics in Signal Processing*, vol. 8, no. 5, pp. 742–758, 2014.

[3] C. D. Altamirano, J. Minango, H. C. Mora, and C. De Almeida, "BER evaluation of linear detectors in massive MIMO systems under imperfect channel estimation effects," *IEEE Access*, vol. 7, pp. 174 482–174 494, 2019.

[4] H. Carvajal, N. Orozco, S. Cacuango, P. Salazar, E. Rosero, and F. Almeida, "A scheduling scheme for improving the performance and security of MU-MIMO systems," *Sensors*, vol. 22, no. 14, Article ID 5369, 2022.

[5] M. Chinnusami, C. V. Ravikumar, S. B. M. Priya et al., "Low complexity signal detection for massive MIMO in B5G uplink system," *IEEE Access*, vol. 11, pp. 91051–91059, 2023.

[6] M. Mulla, A. H. Ulusoy, A. Rizaner, and H. Amca, "A low-complexity iterative algorithm for multiuser millimeter-wave systems," *Annals of Telecommunications*, vol. 79, pp. 101–110, 2024.

[7] H. Q. Ngo, *Massive MIMO: Fundamentals and System Designs*, Vol. 1642, Linköping University Electronic Press, Linköping, Sweeden, 2015.

[8] S. Malkowsky, J. Vieira, L. Liu et al., "The world's first real-time testbed for massive MIMO: design, implementation, and validation," *IEEE Access*, vol. 5, pp. 9073–9088, 2017.

[9] F. A. Pereira de Figueiredo, "An overview of massive MIMO for 5G and 6G," *IEEE Latin America Transactions*, vol. 20, no. 6, pp. 931–940, 2022.

[10] M. D. Yacoub, *Foundations of Mobile Radio Engineering*, CRC Press, New York, NY, 1st edition, 1993.

[11] Y. S. Cho, J. Kim, W. Y. Yang, and C. G. Kang, *MIMO-OFDM Wireless Communications with MATLAB*, John Wiley & Sons, Singapore, 2010.

[12] D. Tse and P. Viswanath, *Fundamentals of Wireless Communication*, Cambridge University Press, Cambridge, UK, 2005.

[13] H. Carvajal and C. de Almeida, "Performance analysis of MC-CDMA systems in Rayleigh fading channel with Inter-cell and co-cell interference," in *2013 IEEE Latin-America Conference on Communications*, pp. 1–6, IEEE, Santiago, Chile, November 2013.

[14] F. A. García, H. Carvajal Mora, and N. O. Garzón, "Improved exact evaluation of equal-gain diversity receivers in Rayleigh fading channels," *IEEE Access*, vol. 10, pp. 26974–26984, 2022.

[15] A. Papoulis, *Probability, Random Variables, and Stochastic Processes*, McGraw-Hill, New York, NY, 4th edition, 2002.

[16] Y. Zhang, M. Zhou, H. Cao, L. Yang, and H. Zhu, "On the performance of cell-free massive MIMO with mixed-ADC under Rician fading channels," *IEEE Communications Letters*, vol. 24, no. 1, pp. 43–47, 2019.

[17] T. Liu, J. Tong, Q. Guo, J. Xi, Y. Yu, and Z. Xiao, "On the performance of massive MIMO systems with low-resolution ADCs and MRC receivers over Rician fading channels," 2019.

[18] J. Arellano, C. D. Altamirano, and H. R. C. Mora, "On the interference reduction factor in massive MIMO system over Rician fading channels," in *2022 IEEE Sixth Ecuador Technical Chapters Meeting (ETCM)*, pp. 1–5, IEEE, Quito, Ecuador, October 2022.

[19] D. N. Amudala, B. Kumar, and R. Budhiraja, "Spatially-correlated Rician-faded multi-relay multi-cell massive MIMO NOMA systems," *IEEE Transactions on Communications*, vol. 70, no. 8, pp. 5317–5335, 2022.

[20] P. Gupta, D. Prajapati, E. Sharma, and D. Ghosh, "Spatially correlated multi-pair massive MIMO relaying with Rician channel and phase shifts," *IEEE Transactions on Vehicular Technology*, vol. 72, no. 4, pp. 4844–4850, 2023.

[21] J. R. Barry, E. A. Lee, and D. G. Messerschmitt, *Digital Communication*, Vol. 1, Kluwer Academic Publishers, Norwell, Massachusetts, USA, 3rd edition, 2004.

[22] S. M. Kay, *Fundamentals of Statistical Signal Processing: Estimation Theory*, Prentice-Hall, Upper Saddle River, NJ, 1993.

[23] A. Tukmanov, J. Weng, and R. Husbands, "Polarization and correlation in MIMO channels," in *WSA & SCC 2023; 26th International ITG Workshop on Smart Antennas and 13th Conference on Systems, Communications, and Coding*, pp. 1–6, VDE, Braunschweig, Germany, February 2023.

[24] L. Sanguinetti, E. Björnson, and J. Hoydis, "Toward massive MIMO 2.0: understanding spatial correlation, interference suppression, and pilot contamination," *IEEE Transactions on Communications*, vol. 68, no. 1, pp. 232–257, 2019.

[25] E. Björnson, J. Hoydis, and L. Sanguinetti, *Massive MIMO Networks: Spectral, Energy, and Hardware Efficiency*, Now Foundations and Trends, 2017.

[26] S.-N. Jin, D.-W. Yue, and H. H. Nguyen, "Proximity co-located massive MIMO systems over correlated Rician fading channels," *Physical Communication*, vol. 49, Article ID 101483, 2021.

[27] P. Liu, D. Kong, J. Ding, Y. Zhang, K. Wang, and J. Choi, "Channel estimation aware performance analysis for massive MIMO with Rician fading," *IEEE Transactions on Communications*, vol. 69, no. 7, pp. 4373–4386, 2021.

[28] P. Liu and T. Jiang, "Channel estimation performance analysis of massive MIMO IoT systems with ricean fading," *IEEE Internet of Things Journal*, vol. 8, no. 7, pp. 6114–6126, 2021.

[29] P. Liu, Q. Zhang, J. Wang, D. Kong, and Y. Zhang, "Statistical description of channel estimation error in massive MIMO systems with ricean fading," *IEEE Transactions on Vehicular Technology*, vol. 70, no. 6, pp. 6227–6231, 2021.

[30] O. Ozdogan, E. Bjornson, and E. G. Larsson, "Uplink spectral efficiency of massive MIMO with spatially correlated Rician fading," in *2018 IEEE 19th International Workshop on Signal Processing Advances in Wireless Communications (SPAWC)*, pp. 1–5, IEEE, Kalamata, Greece, June 2018.

[31] Ö. Özdogan, E. Björnson, and E. G. Larsson, "Massive MIMO with spatially correlated Rician fading channels," *IEEE Transactions on Communications*, vol. 67, no. 5, pp. 3234–3250, 2019.

[32] Z. Wang, J. Zhang, E. Björnson, and B. Ai, "Uplink performance of cell-free massive MIMO over spatially correlated Rician fading channels," *IEEE Communications Letters*, vol. 25, no. 4, pp. 1348–1352, 2021.

[33] A. Adhikary, J. Nam, J.-Y. Ahn, and G. Caire, "Joint spatial division and multiplexing—the large-scale array regime," *IEEE Transactions on Information Theory*, vol. 59, no. 10, pp. 6441–6463, 2013.

[34] P. Maity, S. Srivastava, S. Khatri, and A. K. Jagannatham, "Dictionary-learning (DL)-based sparse CSI estimation in multiuser terahertz (THz) hybrid MIMO systems under hardware impairments and beam-squint effect," *IEEE Access*, vol. 10, pp. 113699–113714, 2022.

[35] H. Yin, D. Gesbert, M. Filippou, and Y. Liu, "A coordinated approach to channel estimation in large-scale multiple-antenna systems," *IEEE Journal on Selected Areas in Communications*, vol. 31, no. 2, pp. 264–273, 2013.

[36] H. Carvajal, N. Orozco, and C. de Almeida, "Performance analysis of MC-CDMA systems employing maximal ratio combining and uniform linear antenna array," in *2014 International Telecommunications Symposium (ITS)*, pp. 1–5, IEEE, Sao Paulo, Brazil, August 2014.

[37] J. Zhang, J. Fan, B. Ai, and D. W. K. Ng, "NOMA-based cell-free massive MIMO over spatially correlated Rician fading channels," in *ICC 2020–2020 IEEE International Conference on Communications (ICC)*, pp. 1–6, IEEE, Dublin, Ireland, June 2020.

[38] J. S. Wallis, "On the existence of Hadamard matrices," *Journal of Combinatorial Theory, Series A*, vol. 21, no. 2, pp. 188–195, 1976.

[39] L. D. Baumert and M. Hall, "Hadamard matrices of the Williamson type," *Mathematics of Computation*, vol. 19, no. 91, pp. 442–447, 1965.

[40] M. Biguesh and A. B. Gershman, "Downlink channel estimation in cellular systems with antenna arrays at base stations using channel probing with feedback," *EURASIP Journal on Advances in Signal Processing*, vol. 2004, Article ID 963649, 2004.

[41] J. H. Kotecha and A. M. Sayeed, "Transmit signal design for optimal estimation of correlated MIMO channels," *IEEE Transactions on Signal Processing*, vol. 52, no. 2, pp. 546–557, 2004.

[42] Y. Liu, T. F. Wong, and W. W. Hager, "Training signal design for estimation of correlated MIMO channels with colored interference," *IEEE Transactions on Signal Processing*, vol. 55, no. 4, pp. 1486–1497, 2007.

[43] K. I. Pedersen, P. E. Mogensen, and B. H. Fleury, "Power azimuth spectrum in outdoor environments," *Electronics Letters*, vol. 33, no. 18, pp. 1583-1584, 1997.

[44] J. D. V. Sánchez, L. Urquiza-Aguiar, and M. C. Paredes Paredes, "Fading channel models for mm-wave Communications," *Electronics*, vol. 10, no. 7, Article ID 798, 2021.

[45] A. Molisch, *Wireless Communications*, John Wiley & Sons, West Sussex, UK, 2nd edition, 2011.